

IMPACT OF RESIDUAL ENERGY ON SOLAR WIND TURBULENT SPECTRA

TREVOR A. BOWEN,^{1,2} ALFRED MALLET,^{3,1} JOHN W. BONNELL,¹ AND STUART D. BALE^{1,2}

¹*Space Sciences Laboratory, University of California, Berkeley, CA*

²*Physics Department, University of California, Berkeley, CA*

³*Space Sciences Center, University of New Hampshire, Durham, NH*

Submitted to ApJ

ABSTRACT

It is widely reported that the power spectra of magnetic field and velocity fluctuations in the solar wind have power law scalings with inertial-range spectral indices of $-5/3$ and $-3/2$ respectively. Studies of solar wind turbulence have repeatedly demonstrated the impact of discontinuities and coherent structures on the measured spectral index. Whether or not such discontinuities are self-generated by the turbulence or simply observations of advected structures from the inner heliosphere has been a matter of considerable debate. This work presents a statistical study of magnetic field and velocity spectral indices over 10 years of solar-wind observations; we find that anomalously steep magnetic spectra occur in magnetically dominated intervals with negative residual energy. However, this increase in negative residual energy has no noticeable impact on the spectral index of the velocity fluctuations, suggesting that these intervals with negative residual energy correspond to intermittent magnetic structures. We show statistically that the difference between magnetic and velocity spectral indices is a monotonic function of residual energy, consistent with previous work which suggests that intermittency in fluctuations causes spectral steepening. Additionally, a statistical analysis of cross helicity demonstrates that when the turbulence is balanced (low cross-helicity), the magnetic and velocity spectral indices are not equal, which suggests that our observations of negative residual energy and intermittent structures are related to non-linear turbulent interactions rather than the presence of advected pre-existing flux-tube structures.

arXiv:1805.02739v1 [astro-ph.SR] 7 May 2018

1. INTRODUCTION

Observations of power law spectral distributions of magnetic and kinetic energy in the solar wind, i.e. $E_\alpha \propto k^\alpha$, have led to the development of various theories of magnetohydrodynamic (MHD) turbulence. It is widely reported that magnetic energy in the inertial range follows a power law spectrum with $E_b \propto k_\perp^{-5/3}$, while kinetic energy follows a shallower power law spectrum of $E_v \propto k_\perp^{-3/2}$ (Mangenev 2001; Salem et al. 2009; Podesta et al. 2007; Borovsky 2012). These spectral indices respectively support the theories of critically balanced turbulence and subsequent modifications accounting for the alignment between velocity and magnetic fluctuations (Goldreich & Sridhar 1995; Boldyrev 2006). The presence of $E \propto k_\perp^{-3/2}$ spectral distributions has been recovered in many subsequent numerical simulations (Perez & Boldyrev 2009; Chandran et al. 2015; Mallet et al. 2017).

It is known that discontinuities and intermittency in observations of turbulence affect measured spectral indices. Roberts & Goldstein (1987) identified large amplitude coherent and discontinuous structures resulting in steep k^{-2} spectra. Li et al. (2011) showed that excluding intermittent current sheets from *Ulysses* magnetometer data led to the measurement of a $E_b \propto k^{-3/2}$ scaling, rather than the typically reported $E_b \propto k^{-5/3}$ scaling. Borovsky (2010) reconstructed the spectral distribution of magnetic field discontinuities of Advanced Composition Explorer (ACE) observations using a synthetic time-series, finding a $E_b \propto k_\perp^{-5/3}$ scaling. There are two dominant explanations for discontinuities and intermittency in the solar wind. The first suggests that discontinuities arise dynamically from the turbulent evolution of the plasma into current sheets (Li et al. 2011; Salem et al. 2009; Mininni & Pouquet 2009; Matthaeus et al. 2015; Boldyrev et al. 2011; Chang et al. 2004). The second suggests that observations of discontinuities correspond to advected flux tube structures from the inner-heliosphere (Tu & Marsch 1993; Borovsky 2008; Mariani et al. 1973; Bruno et al. 2001, 2007).

It is also known that the solar wind contains statistically more magnetic than kinetic energy (Bavassano et al. 1998; Salem et al. 2009; Bruno et al. 1985; Roberts et al. 1987). Various models of MHD turbulence under a range of physical conditions show the growth of negative residual energy, defined as $E_r = E_v - E_b$ (Müller & Grappin 2005; Gogoberidze et al. 2012; Perez & Boldyrev 2009; Boldyrev et al. 2011). The normalized residual energy,

$$\sigma_r = \frac{\langle v^2 \rangle - \langle b^2 \rangle}{\langle v^2 \rangle + \langle b^2 \rangle} = \frac{2\langle \mathbf{z}_+ \cdot \mathbf{z}_- \rangle}{\langle z_-^2 \rangle + \langle z_+^2 \rangle}, \quad (1)$$

is understood to quantify the relative dominance of magnetic or kinetic energy, or equivalently, the alignment between the Elsässer variables defined as $\mathbf{z}_\pm = \mathbf{v} \pm \mathbf{b}/\sqrt{\mu_0\rho_0}$, where \mathbf{v} and \mathbf{b} are the fluctuating velocity and magnetic fields and ρ_0 is the mean mass density.

A power law spectrum for E_r was derived by Grappin et al. (1983), with $E_r \propto k^{-2}$ under the assumption of weak turbulence. Müller & Grappin (2005) have subsequently suggested $E_r \propto k^{-7/3}$ spectra for decaying isotropic turbulence and $E_r \propto k^{-2}$ scaling for forced anisotropic turbulence. Chen et al. (2013) used a statistical study of *Wind* observations to explore connections between spectral index and residual energy, reporting a mean value of $\alpha_r = -1.91$ and a significant correlation between α_r and α_b . In a study demonstrating scale invariance of normalized cross helicity

$$\sigma_c = \frac{2\langle \delta\mathbf{b} \cdot \delta\mathbf{v} \rangle}{\langle v^2 \rangle + \langle b^2 \rangle} = \frac{\langle z_+^2 \rangle - \langle z_-^2 \rangle}{\langle z_-^2 \rangle + \langle z_+^2 \rangle}, \quad (2)$$

Podesta & Borovsky (2010) reported $\alpha_r = -1.75$. Both studies demonstrate correlations between cross helicity and spectral indices for magnetic fields, velocity, as well as total energy.

The connection between cross helicity and residual energy is well established. Bruno et al. (2007) show that as fast solar wind evolves from 0.3 -1AU the distribution of *Helios* measurements moves from a highly cross helical (imbalanced) state to a state with low cross helicity (balanced) and high negative residual energy. Wicks et al. (2013a) studied the evolution of cross helicity and residual energy over injection and inertial scales, arguing that the mean angle between the Elsässer variables is scale dependent and maximized at the outer scale. Wicks et al. (2013b) show that observations of turbulence tend to be either strongly cross helical, or have strong residual energy.

In this Letter, we use 10 years of *Wind* observations to study statistical connections between intermittency, magnetic discontinuities, residual energy, and spectral index. We demonstrate that discontinuous events are associated with magnetically dominated intervals with large negative residual energies. Intermittent discontinuities steepen the magnetic spectral index, but have little effect on the measured velocity spectra. Our observations are consistent with the generation of residual energy and intermittency through turbulence, and suggest a close link between residual energy and intermittency.

2. DATA

We use observations from several instruments on the *Wind* mission ranging 1996 January 1 through 2005 December 31: Magnetic Field Investigation (MFI) Lepping

et al. (1995), Solar Wind Experiment (SWE) Ogilvie et al. (1995), and Three Dimensional Plasma (3DP) experiment Lin et al. (1995). Data are separated into non-overlapping 1 hr intervals. Intervals are excluded if any of several conditions are met: *Wind's* geocentric distance is less than $35R_E$, the average solar wind speed is < 250 km/s, or if more than 5% of observations are missing from any one instrument. Linear interpolation is implemented across small data gaps when $< 5\%$ of an interval is missing. The resulting data consists of 39415 intervals of 1 hour.

The 3 s cadence 3DP “on board” proton moment measurements are interpolated to the MFI time base. We separate velocity, and magnetic field measurements (\mathbf{v} , and \mathbf{B}) into mean and fluctuation quantities using time-averaged values, denoted as $\langle \dots \rangle$. For example, the mean magnetic field, \mathbf{B}_0 , is determined by $\langle \mathbf{B} \rangle = \mathbf{B}_0$ with the fluctuation quantities as $\delta \mathbf{B} = \mathbf{B} - \mathbf{B}_0$. We normalize the magnetic field to Alfvén units using $\delta \mathbf{b} = \delta \mathbf{B} / \sqrt{\mu_0 \rho_0}$ where ρ_0 is the mean mass density.

Each interval is characterized by energies associated with the velocity and magnetic field fluctuations $E_b = \frac{1}{2} \langle \delta b^2 \rangle$ and $E_v = \frac{1}{2} \langle \delta v^2 \rangle$, normalized cross helicity,

$$\sigma_c = \frac{2 \langle \delta \mathbf{b} \cdot \delta \mathbf{v} \rangle}{\langle \delta b^2 \rangle + \langle \delta v^2 \rangle}, \quad (3)$$

and normalized residual energy

$$\sigma_r = \frac{E_v - E_b}{E_v + E_b}. \quad (4)$$

A minimum variance analysis (MVA) is performed on $\delta \mathbf{v}$ and $\delta \mathbf{b}$ to decompose each interval into eigenvectors corresponding to directions of minimum, maximum, and intermediate variance (Sonnerup & Cahill 1967). Intervals with maximum energy is largely distributed along a single direction, i.e. if $\lambda_b^{max} \approx E_b$, may indicate the presence of strong discontinuities or a linear polarization to the fluctuations (Bruno et al. 2001).

Intermittency in the magnetic field is often associated with current sheets Matthaeus et al. (2015); Veltri & Mangeney (1999); Mininni & Pouquet (2009); Mallet et al. (2016). Using Ampere’s law

$$\nabla \times \mathbf{B} = \mu_0 \mathbf{J} \quad (5)$$

and invoking the Taylor hypothesis, $\frac{\partial}{\partial t} \sim \mathbf{V} \cdot \nabla$ allows the time derivative of magnetic field observations in the spacecraft frame to be used as a proxy for current (Podesta & Roytershteyn 2017). Because single spacecraft observations constrain spatial derivatives to the bulk solar wind flow direction, the full curl cannot be computed. To estimate the magnitude of currents we

implement the reduced curl

$$\nabla_x \times \mathbf{B} = -\frac{\partial}{\partial x} B_z \hat{y} + \frac{\partial}{\partial x} B_y \hat{z}, \quad (6)$$

where the solar wind flow is along \hat{x} . Applying the Taylor hypothesis gives an estimate of the current magnitude,

$$J = \frac{1}{\mu_0 V_{sw}} \sqrt{\left(\frac{\partial B_y}{\partial t}\right)^2 + \left(\frac{\partial B_z}{\partial t}\right)^2}. \quad (7)$$

A reduced estimate for the vorticity magnitude $\omega = \nabla \times \mathbf{v}$ is similarly computed.

Intermittency is frequently quantified using the kurtosis,

$$\kappa_x = \frac{\langle x^4 \rangle}{\langle x^2 \rangle^2} \quad (8)$$

(Bruno et al. 2001, 2003; Salem et al. 2009; Mangeney 2001; Veltri & Mangeney 1999; Frisch & Kolmogorov 1995; Matthaeus et al. 2015). Gaussian distribution have $\kappa = 3$, with $\kappa > 3$ indicating heavy tailed, non-Gaussian statistics. As a simple statistic to quantify intermittency in the magnetic and velocity fluctuations we measure the kurtosis of the reduced curl estimations of the current and vorticity, κ_J and κ_ω for each interval, subtracting 3 to compare with Gaussian statistics.

3. SPECTRAL FITTING

Trace spectral indices for the magnetic and velocity fluctuations in the inertial turbulent range are estimated by performing a linear least squares fit of the power spectra to a line in logarithmic space. Power spectra for $\mathbf{b}(t)$ and $\mathbf{v}(t)$ are estimated with a fast-Fourier transform. The trace power spectra, \tilde{E}_b and \tilde{E}_v are calculated as the sum power spectra from each direction axis.

To prevent overlapping with injection scales, our fits only consider frequencies above ~ 0.277 Hz (6 minutes). To avoid spectral steepening associated with the dissipative scales at high frequencies, we only consider the subsequent 190 frequency bins (up to 0.0555 Hz, or 18 seconds). The trace spectra are linearly interpolated to an abscissa of 50 logarithmically spaced frequencies (linearly spaced in the logarithmic domain) between 0.277-0.0555 Hz. The power spectra is estimated using a linear least square fit of the interpolated spectra and frequencies in log-log space, with the slope of the best fit line giving the spectral index (Podesta 2016; Chen et al. 2013). The spectral index of the trace residual energy is calculated from fitting $|\tilde{E}_r| = |\tilde{E}_v - \tilde{E}_b|$ with the same interpolation and least square fitting scheme. Additionally, the high frequency limit helps to minimize flattening effects due Gaussian noise in low amplitude 3DP velocity measurements; though the range of our spectral

fits extends to slightly higher frequencies than what previous authors have used, we find good agreement with their estimates for mean values of α_v and α_b (Chen et al. 2013; Wicks et al. 2013a; Podesta & Borovsky 2010).

Uncertainty of our estimated spectral indices is found through propagation of error (Press et al. 1992). The variance associated with single FFT estimation of spectral density is equal to the power spectral density itself. Typically, variance is reduced through averaging over an ensemble of spectra, or windowing the autocorrelation function of a time-series. Here we derive the uncertainty in spectral index associated with least squares fitting of a single FFT estimation of spectral density. For spectral density S_i where index i refers to a given frequency bin, f_i , Stoica & Moses (2005) give the variance of the spectral density as

$$\text{Var}[S_i] = \sigma_i^2 \approx S_i^2. \quad (9)$$

Propagating the variance σ_i^2 to the logarithm of the spectral density $\log_{10}(S_i)$ gives

$$\text{Var}[\log_{10}S_i] = \sigma_L^2 = \left(\frac{1}{\ln 10}\right)^2 \frac{\sigma_i^2}{S_i^2} \approx 0.19. \quad (10)$$

The scaling of $\text{Var}[\tilde{S}_i] = S_i$ leads to constant variance in the estimation of the logarithm of spectral density.

For a power law spectra $S_i = \beta f_i^\alpha$ minimizing

$$\chi^2 = \sum_{i=0}^{N-1} \left(\frac{y_i - \beta - \alpha x_i}{\sigma_L}\right)^2, \quad (11)$$

where $y_i = \log_{10}S_i$ and $x_i = \log_{10}f_i$, with respect to α and β gives the least square best fits for the spectral index and scaling amplitude. Following Press et al. (1992) for propagation of errors gives the uncertainty in α as

$$\sigma_\alpha^2 = \sum_i \left(\frac{\partial \alpha}{\partial y_i}\right)^2 \sigma_L^2 = \sigma_L^2 \frac{\sum x_i^2}{N \sum x_i^2 - (\sum x_i)^2}. \quad (12)$$

The uncertainty in the estimated spectral index, a function of σ_L^2 and the uniformly used frequency abscissa, is constant for each interval with $\sigma_\alpha = \pm 0.16$.

4. RESULTS

Figure 1 shows the probability distributions of α_b , α_v , and α_r , with respective means of -1.66, -1.47, and -1.73. Our fits for the the velocity and magnetic energy spectra agree with spectral indices given in previous studies (Mangeney 2001; Salem et al. 2009; Podesta et al. 2007; Borovsky 2012). The mean value of α_r slightly shallower than observations in Chen et al. (2013) but is consistent with Podesta & Borovsky (2010). Our observations of

α_r are also shallower than predictions of various models of MHD turbulence (Grappin et al. 1983; Müller & Grappin 2005; Gogoberidze et al. 2012); however, these models are conducted using assumptions which are not satisfied by solar wind turbulence, e.g. weak turbulence, isotropy, and quasi-normal closure. Deviation in our measurements of α_r from Chen et al. (2013) likely occur due to differences in the fitting technique and normalization of the magnetic field. Our work directly fits \tilde{E}_r as the difference in observed velocity and magnetic spectra, and implements MHD normalization of the magnetic field. Chen et al. (2013) use fitted spectra to calculate α_r and implement a kinetic normalization of the magnetic field. The right panels of Figure 1 show examples of \tilde{E}_b , \tilde{E}_v , and \tilde{E}_r with our fits.

The left panel of Figure 2 shows the joint distribution of α_b and α_v . The mean value of the velocity spectral index is $\alpha_v = -3/2$. A tendency for $\alpha_b < \alpha_v$ is evident in the distribution. The right panel of Figure 2 shows the joint distribution of magnetic and velocity indices colored by the mean value of σ_r . The statistical preference for negative residual energy is clearly evident in our observations. The residual energy becomes more negative as the spectral indices α_v and α_b diverge, i.e. as the magnetic spectral index steepens. Particularly interesting is the consistent level of residual energy along the line $\alpha_v = \alpha_b$ throughout the range of observations.

The left panel of Figure 3 shows the joint distribution of σ_r and α_b . The secular trend suggests that the residual energy plays a significant role in setting the spectral index of the magnetic field. Specifically, it is evident that magnetically dominated intervals, with $\sigma_r \approx -1$, exhibit steeper magnetic spectra. The right panel of Figure 3 shows the joint distribution of α_r and α_b , these variables are highly correlated with a Pearson correlation value of 0.78. A linear best fit gives $\alpha_b \propto 0.56\alpha_r$. These results imply that spectral indices of the magnetic fluctuations and residual energy are largely determined by the average residual energy over each interval.

The left panel of Figure 4 shows the joint distribution of σ_r and α_v . Unlike the spectral index of the magnetic fluctuations, α_v exhibits little dependence on σ_r , suggesting that residual energy is mostly determined by magnetic fluctuations. The middle panel of Figure 4 shows the difference between the magnetic and velocity spectral indices as a function of residual energy. As the residual energy increases, i.e. the plasma becomes less magnetically dominated, the spectral index of the magnetic field approaches that of the velocity spectra.

The right panel of Figure 4 shows the joint distribution of the difference between magnetic and velocity spectral indices, $\alpha_v - \alpha_b$, and cross helicity, σ_c , suggesting

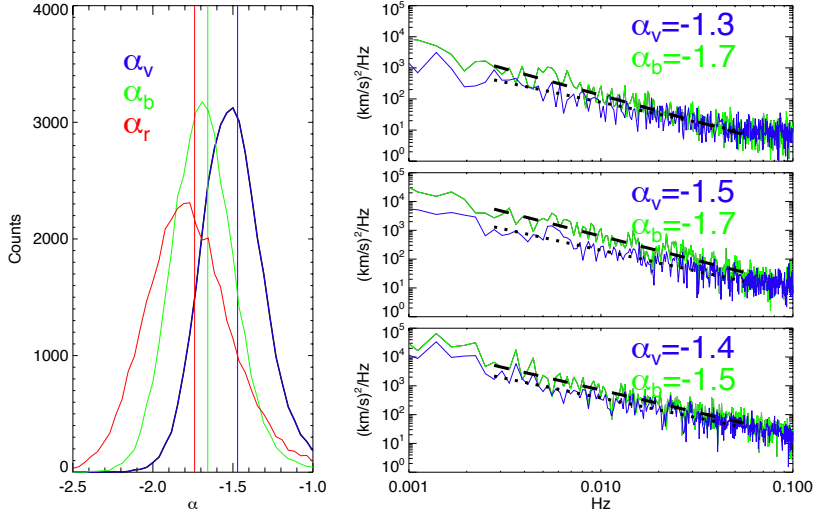


Figure 1. (Left) Distribution of fits power-law indices for magnetic field (green), velocity (blue), and residual energy (red) spectra, mean values are shown with vertical lines. (Right) Examples of measured magnetic field (in Alfvén units) and velocity fluctuation spectra. Fits for the magnetic and velocity spectra are shown respectively as black dashed and dotted lines.

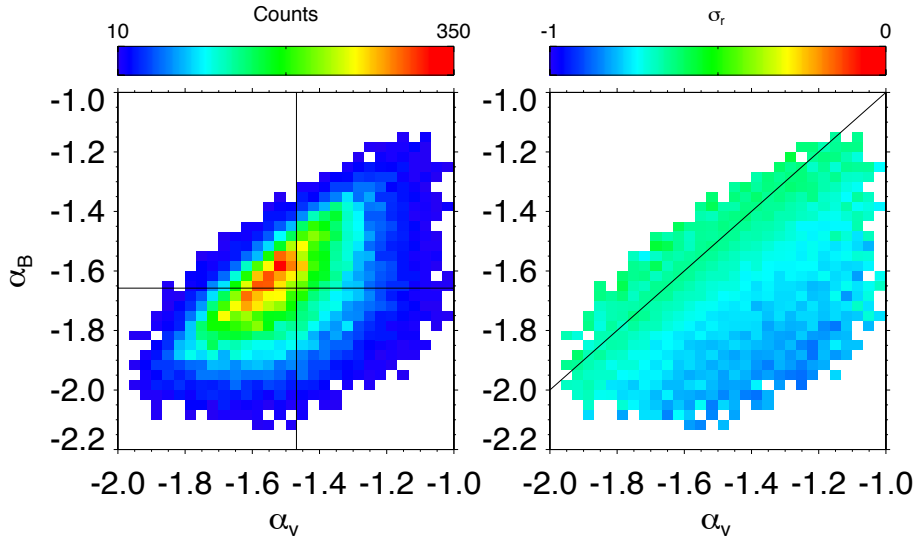


Figure 2. (Left) Joint distribution of the fitted spectral indices for magnetic field, α_b , and velocity, α_v , fluctuations in the inertial range. The black lines show the mean values of $\alpha_v \sim -3/2$ and $\alpha_b \sim -5/3$. (Right) The distribution of α_v and α_b colored by the mean residual energy in each bin. The black line shows $\alpha_v = \alpha_b$. Deviations from $\alpha_v \approx \alpha_b$ lead to an increase in negative residual energy ($E_b > E_v$).

that high cross helicity measurements occur only when $\alpha_v = \alpha_b$. A geometrical consideration of cross helicity and residual energy gives the constraint of $\sigma_c^2 + \sigma_r^2 < 1$ (Wicks et al. 2013b). Clearly, the decrease of $|\sigma_c|$ with large negative σ_r and $|\alpha_b| > |\alpha_v|$ is inevitable. However, there is no such geometric argument which demands balanced turbulence (i.e. $|\sigma_c| < 1$) to coincide with unequal spectral indices such that $\alpha_b \neq \alpha_v$. The observations in Figure 4 (Right), in which the joint distribution of

$\alpha_v - \alpha_b$ is conditioned on σ_c suggests that balanced turbulence (i.e. $|\sigma_c| < 1$) coincides with $|\alpha_b| > |\alpha_v|$. There is no *a priori* reason that we expect balanced turbulence (i.e. $|\sigma_c| < 1$) to have different spectral indices, $\alpha_b \neq \alpha_v$. This result is consistent with the generation of negative residual energy through turbulence, i.e. that non-linear interactions between the Elsässer variables lead to the growth of intermittent structures with negative residual

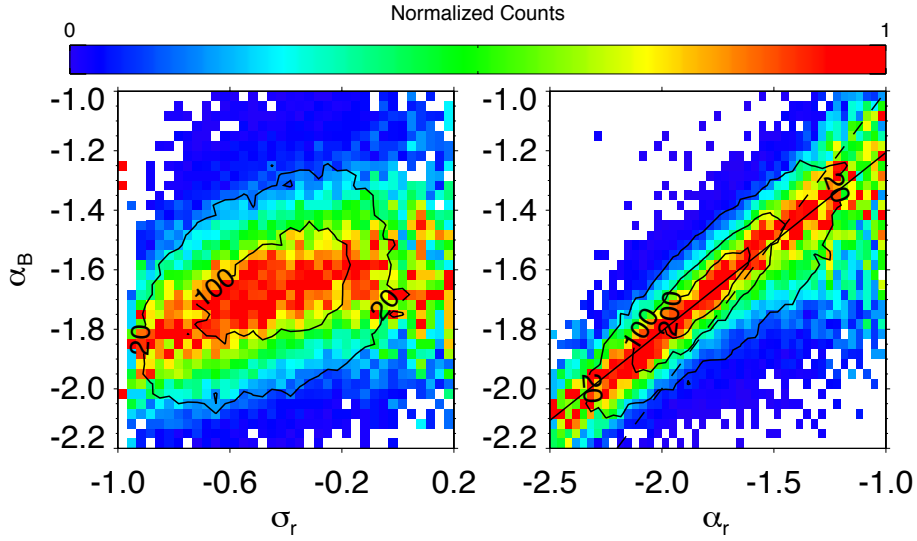


Figure 3. (Left) Joint distribution of normalized residual energy σ_r and spectral index of the inertial range magnetic fluctuations α_b . Data is column normalized to the maximum number of counts in each σ_r bin. (Right) Joint distributions of fitted power law spectral indices of residual energy spectra α_r and inertial range magnetic field fluctuations α_b . The solid black line shows the least square linear fit to the data with correlation 0.77 and slope of 0.56. The dashed line shows $\alpha_r = \alpha_b$. Contours in either panel show 20, 100, and 200 level counts of the joint distributions.

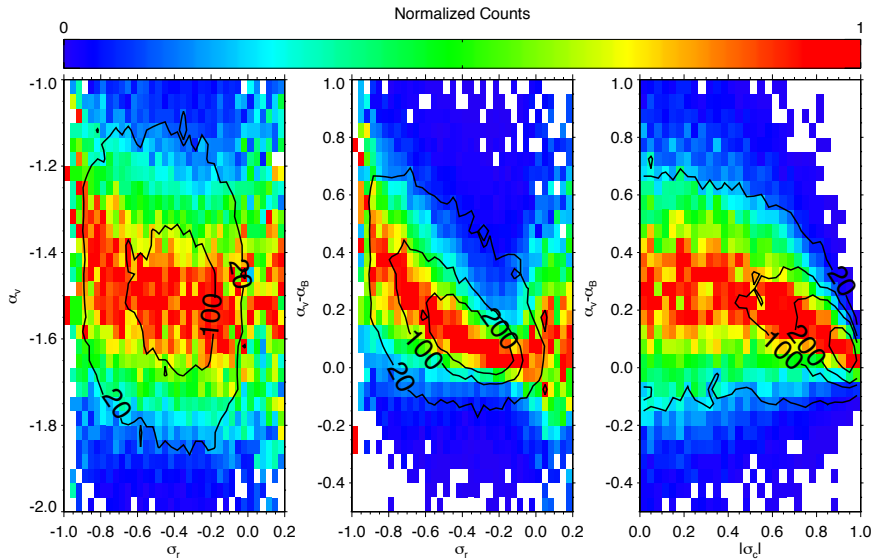


Figure 4. (Left) Joint distribution of fit velocity spectral index α_v with root-mean-square residual energy σ_r . The distribution is column normalized to the maximum occurrence of α_v for each value of σ_r . (Center) Joint distribution of the difference in velocity and magnetic field spectral indices, $\alpha_v - \alpha_b$, with σ_r . (Right) Joint distribution of the difference in velocity and magnetic field spectral indices, $\alpha_v - \alpha_b$, with σ_c . Data is column normalized to the maximum number of counts of $\alpha_v - \alpha_b$ in each bin of σ_c . Contours in all three plots show 20, 100, and 200 count levels of the distributions.

energy, since at fixed total energy the nonlinear interaction term $\mathbf{z}_\pm \cdot \nabla \mathbf{z}_\mp$ are stronger when $\sigma_c = 0$.

Using the MVA analysis, the value λ^{max} corresponding the fraction of energy associated with the maximum variance direction, is calculated for both the magnetic and velocity fluctuations. The top panels of Figure 5 show the joint distributions of λ_b^{max} (Left) and λ_v^{max} (Right) with the residual energy. There is a strong dependence of λ_b^{max} on the residual energy which is not observed for λ_v^{max} . This suggests that large negative residual energy occurs as the result of discontinuous/coherent structures in the magnetic field. In fact, the most negative values of residual energy seem to demonstrate the smallest values of λ_v^{max} , which suggest more isotropic velocity fluctuations; however, this could be due to sampling bias towards very low amplitude velocity fluctuations subject to noise.

To further connect the negative residual energy with magnetic intermittency, we examine the kurtosis of the reduced curl estimates for current and vorticity, κ_J and κ_ω , as proxies for intermittent features. The bottom panels of Figure 5 show the joint distribution of the residual energy and κ_J . A decrease in κ_J is observed with increasing residual energy, suggesting that the negative residual energy is caused by magnetic discontinuities with associated bursty currents. At low residual energy the velocity fluctuations appear more Gaussian, which may indicate very low amplitude velocity fluctuations possibly subject to noise. Regardless, we uniformly observe $\kappa_\omega < \kappa_J$, suggesting less intermittency in the velocity fluctuations.

5. DISCUSSION

Many authors recover $k^{-3/2}$ spectra in simulations (Maron & Goldreich 2001; Müller & Grappin 2005; Perez & Boldyrev 2009; Mallet et al. 2016). This scaling is in agreement with analytic predictions of strong, three dimensional, anisotropic, turbulence appropriate for the solar wind (Boldyrev 2006; Chandran et al. 2015; Mallet & Schekochihin 2017; Bruno & Carbone 2013). Our observations here suggest that the observed difference between the spectral indices of velocity and magnetic field turbulent fluctuations occurs due to the presence of negative residual energy in the form of intermittent current sheets. When the magnetic and velocity energies are in equipartition, the spectral slope of the magnetic fluctuations approaches the velocity spectral index. The velocity spectral index is insensitive to the residual energy with a mean value of $\alpha_v = -3/2$. This picture is consistent with the numerical model of Mininni & Pouquet (2009), which demonstrates the formation of thin current sheets in the magnetic field through decay-

ing turbulence leading to enhanced intermittency and steepening of magnetic spectral index of $\alpha_b = -5/3$. In this interpretation, the magnetic fluctuations form thinner structures than the velocity fluctuations, which then dissipate energy more quickly. This picture does not address the collisionless and kinetic nature of dissipation in the solar wind; a full explanation requires a more complex account of the physical mechanisms of dissipation.

Our results are congruent with Li et al. (2011) who interpreted their results as indicative of flux-tube crossings. However, for several reasons, we believe our results support the idea of intermittency through turbulence rather than observations of advected flux tubes. First, we have identified the presence of intermittent events in the magnetic field contributing to negative residual energy which have no accompanying signature in the velocity fluctuations. Observed intervals with intermittent signatures present in both velocity and magnetic fluctuations are likely contained along the $\alpha_v = \alpha_b$ line, where steepening may occur in both the magnetic and velocity spectra. If observations of flux tube crossings are present in the dataset, they likely exist in this region. Additionally, our results agree with Salem et al. (2009) who note that the high kurtosis distributions which affect measurements of spectral indices occur at lower fluctuation amplitudes in the magnetic field than in the velocity measurements. This again suggests the presence of intermittent magnetic fluctuations with no velocity component.

The joint distribution of the difference of spectral slopes, $\alpha_v - \alpha_b$, and the cross helicity σ_c , suggests that intervals of balanced turbulence preferentially occur with $\alpha_v \neq \alpha_b$. Though unequal spectral slopes, associated with non-equipartitioned E_v and E_b , geometrically preclude the observation of imbalanced fluctuations with $|\sigma_c| \sim 1$, the observations in Figure 4 (Right) suggest the stronger statement that balanced turbulence occurs only with unequal spectral indices. We interpret the lack of balanced turbulence with $\alpha_v = \alpha_b$ as evidence for the generation of residual energy through non-linear turbulent interactions (Boldyrev et al. 2011). The observation that solar wind turbulence is either highly imbalanced, $|\sigma_c| = 1$ or highly anti-aligned $\sigma_r = -1$ has been noted by previous authors (Wicks et al. 2013b; Bruno et al. 2007); however, observations of low cross helicity directly corresponding directly to deviations in turbulent spectral indices suggests that the residual energy is closely connected with non-linear turbulent interactions.

The quantification of the variance in spectral density estimates demonstrates that our fit spectral indices are accurate to 10%. The implementation of this variance

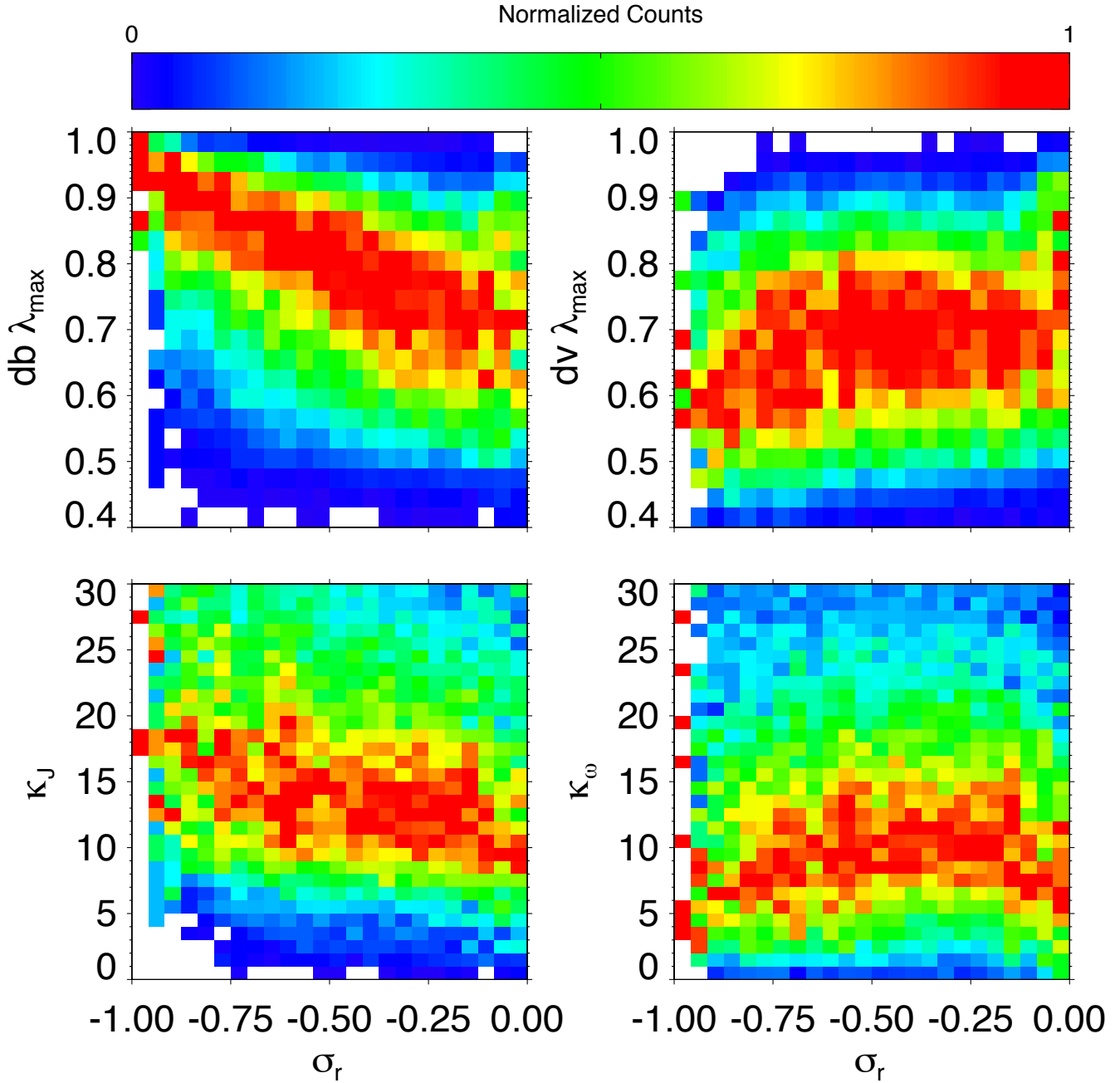


Figure 5. (Top Left) Joint distribution of maximum normalized eigenvalue of magnetic field fluctuations, λ_b^{max} , with σ_r . Large negative residual energy corresponds with large λ_b^{max} . The joint distribution of λ_v^{max} with the residual energy (Top Right) does not show a dependence on the residual energy. Joint distributions of the kurtosis of reduced current (Bottom Left) and vorticity (Bottom Right) with residual energy show that negative residual energy corresponds to intermittent currents with no associated signature in the velocity fluctuations.

estimate will help constrain observations made of the inner heliosphere by the *FIELDS* instrument on the Parker Solar Probe (Bale et al. 2016). Additionally, a quantitative characterization of spectral index variance may prove useful in further studies of *Wind* observations, e.g. determining the nature compressive fluctuations in the solar wind (Bowen et al. 2018).

6. ACKNOWLEDGEMENTS

A. Mallet would like to acknowledge useful conversation with B.D.G. Chandran and A.A. Schekochihin. T.A.B. was supported by NASA Earth and Space Science Fellowship NNX16AT22H. A. Mallet was supported by NSF grant AGS-1624501. *Wind*/3DP data analysis at UC Berkeley is supported in part by NASA grant NNX16AP95G.

REFERENCES

- Bale, S. D., Goetz, K., Harvey, P. R., et al. 2016, *SSRv*, 204, 49
- Bavassano, B., Pietropaolo, E., & Bruno, R. 1998, *J. Geophys. Res.*, 103, 6521
- Boldyrev, S. 2006, *Physical Review Letters*, 96, 115002
- Boldyrev, S., Perez, J. C., Borovsky, J. E., & Podesta, J. J. 2011, *ApJL*, 741, L19
- Borovsky, J. E. 2008, *Journal of Geophysical Research (Space Physics)*, 113, A08110
- . 2010, *Physical Review Letters*, 105, 111102
- . 2012, *Journal of Geophysical Research (Space Physics)*, 117, A05104
- Bowen, T. A., Badman, S., Hellinger, P., & Bale, S. D. 2018, *ApJL*, 854, L33
- Bruno, R., Bavassano, B., & Villante, U. 1985, *J. Geophys. Res.*, 90, 4373
- Bruno, R., & Carbone, V. 2013, *Living Reviews in Solar Physics*, 10, 2
- Bruno, R., Carbone, V., Sorriso-Valvo, L., & Bavassano, B. 2003, *Journal of Geophysical Research (Space Physics)*, 108, 1130
- Bruno, R., Carbone, V., Veltri, P., Pietropaolo, E., & Bavassano, B. 2001, *Planet. Space Sci.*, 49, 1201
- Bruno, R., D’Amicis, R., Bavassano, B., Carbone, V., & Sorriso-Valvo, L. 2007, *Annales Geophysicae*, 25, 1913
- Chandran, B. D. G., Schekochihin, A. A., & Mallet, A. 2015, *ApJ*, 807, 39
- Chang, T., Tam, S. W. Y., & Wu, C.-C. 2004, *Physics of Plasmas*, 11, 1287
- Chen, C. H. K., Bale, S. D., Salem, C. S., & Maruca, B. A. 2013, *ApJ*, 770, 125
- Frisch, U., & Kolmogorov, A. 1995, *Turbulence: The Legacy of A. N. Kolmogorov* (Cambridge University Press)
- Gogoberidze, G., Chapman, S. C., & Hnat, B. 2012, *Physics of Plasmas*, 19, 102310
- Goldreich, P., & Sridhar, S. 1995, *ApJ*, 438, 763
- Grappin, R., Leorat, J., & Pouquet, A. 1983, *A&A*, 126, 51
- Lepping, R. P., Acuña, M. H., Burlaga, L. F., et al. 1995, *SSRv*, 71, 207
- Li, G., Miao, B., Hu, Q., & Qin, G. 2011, *Physical Review Letters*, 106, 125001
- Lin, R. P., Anderson, K. A., Ashford, S., et al. 1995, *SSRv*, 71, 125
- Mallet, A., & Schekochihin, A. A. 2017, *MNRAS*, 466, 3918
- Mallet, A., Schekochihin, A. A., & Chandran, B. D. G. 2017, *MNRAS*, 468, 4862
- Mallet, A., Schekochihin, A. A., Chandran, B. D. G., et al. 2016, *MNRAS*, 459, 2130
- Mangency, A. 2001, in *ESA Special Publication*, Vol. 492, *Sheffield Space Plasma Meeting: Multipoint Measurements versus Theory*, ed. B. Warmbein, 53
- Mariani, F., Bavassano, B., Villante, U., & Ness, N. F. 1973, *J. Geophys. Res.*, 78, 8011
- Maron, J., & Goldreich, P. 2001, *ApJ*, 554, 1175
- Matthaeus, W. H., Wan, M., Servidio, S., et al. 2015, *Philosophical Transactions of the Royal Society of London Series A*, 373, 20140154
- Mininni, P. D., & Pouquet, A. 2009, *PhRvE*, 80, 025401
- Müller, W.-C., & Grappin, R. 2005, *Physical Review Letters*, 95, 114502
- Ogilvie, K. W., Chornay, D. J., Fritzenreiter, R. J., et al. 1995, *SSRv*, 71, 55
- Perez, J. C., & Boldyrev, S. 2009, *Physical Review Letters*, 102, 025003
- Podesta, J. J. 2016, *Advances in Space Research*, 57, 1127
- Podesta, J. J., & Borovsky, J. E. 2010, *Physics of Plasmas*, 17, 112905
- Podesta, J. J., Roberts, D. A., & Goldstein, M. L. 2007, *ApJ*, 664, 543
- Podesta, J. J., & Roytershteyn, V. 2017, *Journal of Geophysical Research (Space Physics)*, 122, 6991
- Press, W. H., Teukolsky, S. A., Vetterling, W. T., & Flannery, B. P. 1992, *Numerical Recipes in C (2Nd Ed.): The Art of Scientific Computing* (New York, NY, USA: Cambridge University Press)

- Roberts, D. A., & Goldstein, M. L. 1987, *J. Geophys. Res.*, 92, 10
- Roberts, D. A., Klein, L. W., Goldstein, M. L., & Matthaeus, W. H. 1987, *J. Geophys. Res.*, 92, 11021
- Salem, C., Mangeney, A., Bale, S. D., & Veltri, P. 2009, *ApJ*, 702, 537
- Sonnerup, B. U. O., & Cahill, Jr., L. J. 1967, *J. Geophys. Res.*, 72, 171
- Stoica, P., & Moses, R. 2005, *Spectral Analysis of Signals* (Pearson Prentice Hall)
- Tu, C.-Y., & Marsch, E. 1993, *J. Geophys. Res.*, 98, 1257
- Veltri, P., & Mangeney, A. 1999, in *American Institute of Physics Conference Series*, Vol. 471, American Institute of Physics Conference Series, ed. S. R. Habbal, R. Esser, J. V. Hollweg, & P. A. Isenberg, 543–546
- Wicks, R. T., Mallet, A., Horbury, T. S., et al. 2013a, *Physical Review Letters*, 110, 025003
- Wicks, R. T., Roberts, D. A., Mallet, A., et al. 2013b, *ApJ*, 778, 177